J. Mod. Transport. (2015) 23(4):287–297
DOI 10.1007/s40534-015-0087-x

CrossMark

An analytic study on the deflection of subway tunnel due to adjacent excavation of foundation pit

Zelin Zhou[1] · Shougen Chen[1] · Peng Tu[1] · Haisheng Zhang[1]

Received: 5 March 2015 / Revised: 21 October 2015 / Accepted: 23 October 2015 / Published online: 19 November 2015

Abstract Predicting and estimating the response of subway tunnel to adjacent excavation of foundation pit is a research focus in the field of underground engineering. Based on the principle of two-stage method and incremental method, an analytic approach is suggested in this paper to solve this problem in an accurate and rapid way, and the upheavals of tunnel due to adjacent excavation are solved by analytic method. Besides, the presented method is used in the practical engineering case of Shenzhen Metro Line 11 and verified by numerical simulation and in situ measurement. Finally, a parametric analysis is performed to investigate the influence of different factors on tunnel's deflection. Some useful conclusions have been drawn from the research as below: The deflection results of tunnel obtained from analytic method are nearly consistent with the results getting from numerical analysis and measured data, which verified the accuracy and rationality of presented method. The excavation size has a significant impact on both the displacement values and influenced range of tunnel. However, the relative distance only impacts the displacement values of tunnel, but not the influenced range of tunnel. It may provide certain reference to analyze the deflection of subway tunnel influenced by adjacent excavation.

Keywords Subway tunnel · Upheaval deflection · Excavation of foundation pit · Two-Stage Method · Parametric analysis

✉ Zelin Zhou
zhouzelin2016@163.com

[1] Key Laboratory of Transportation Tunnel Engineering, Ministry of Education, School of Civil Engineering, Southwest Jiaotong University, Chengdu 610031, China

1 Introduction

With the rapid development of urban underground space, more and more excavations adjacent to underground space are constructed, in which the soil unloading due to adjacent excavations will lead to an uplift of underlying tunnels. As a life line of the city transport, the criterion of allowable deflection of subway tunnels is very strict. According to the design code of building foundation in China, the uplift of existing subway tunnels cannot be bigger than 10.0 mm, while the deflection radius cannot be less than 15,000.0 m. A typical case to damage a tunnel in the Pachiao line due to nearby excavations in Taipei caused a big loss [1]. Therefore, effectively predicting the tunnel deflection in such cases is very important in order to reduce the risk and has recently become a big concern in underground constructions.

Many cases of interaction behavior between excavations and existing tunnels have been studied using numerical modeling and analytical studies. For example, Dolezalova [2] used a 2D numerical model to analyze the deformation of a tunnel underlying a deep-open excavation. Gao et al. [3] investigated the influence of excavations on a nearby road tunnel using 3D FEM. Hu et al. [4] used FEM to investigate the deformation of subway tunnels due to adjacent pit excavations. The numerical modeling is powerful to deal with the pit excavation steps and can consider nonlinear interactions between tunnels and surrounding soil. However, the reliability of the modeling result depends greatly on the constitutive model and hypothetic material parameters.

In general, the analytical method allows a convenient and rapid approach to estimate the tunnel deflection for engineers. Ji et al. [5] presented a simple analytical method, which is called residual stress method (RSM), to analyze the tunnel displacement induced by adjacent excavations, but it cannot consider the effect of tunnel stiffness. Zhang et al. [6] proposed a two-stage method based on elasticity theory to examine the influence of adjacent pit excavations on existing tunnels. First, the elasticity solution is used to compute the soil stress due to adjacent excavations. By simplifying the existing tunnel as a continuous foundation beam, an analytical formula can be derived to solve the tunnel deflection. The two-stage method has been verified in actual projects and recently attracts a growing research attention, particularly in the deformation prediction for tunnels and pipelines due to adjacent pit excavations [7, 8]. However, the two-stage method has some problems which deserve further studies. First, most studies focused on the vertical load released from the bottom of pits and no horizontal released load from the sidewalls of the pits is considered. The influence of support structures of pits such as retaining walls and lateral braces is often neglected. Second, in simulating the interaction between tunnels and surrounding soil, the traditional Winkler' foundation model using a series of separate spring elements to reflect the soil is usually adopted in most studies. Although the Winkler' foundation model has its own advantages, it is unable to consider the soil continuity so that the tunnel deflection cannot be obtained accurately.

Based on the principle of two-stage method, this study aims to predict the tunnel deflection due to adjacent pit excavations more accurately and rapidly. First, the unloading soil stress due to adjacent excavations is computed based on the Mindlin' elastic theory. By taking account of support structures, the incremental method is adopted to analyze the interaction between the support structure and soil. Second, the governing differential equation for the tunnel is established by assuming the tunnel being a continuous beam on Pasternak' foundation. Then the differential equation is derived to obtain the analytical solution. Moreover, the proposed method is applied to a project case to study the deflection pattern of adjacent double-hole tunnels. The analytical result is compared with numerical modeling and monitoring results to examine the reliability of the proposed method. Finally, a parametric study was also performed to examine major influential factors on the tunnel deflection including the pit excavation size and relative distance between the tunnels and the excavation.

2 Derivation of the analytical solution

A deep pit excavation above a tunnel breaks the mechanical balance and generates a released load from the pit. The released load then causes a stress redistribution and deformation surrounding the tunnel.

2.1 Establishment of the analytical model

The analytical model for deriving the deflection of an existing tunnel due to an adjacent pit excavation is shown in Fig. 1. A 3D-Cartesian coordinate system is established at the center of foundation pit. The pit excavation is B, L, and H, in width, length, and height, respectively.

As shown in Fig. 1, there are five stress unloading faces after the pit excavation, i.e., one bottom face numbered as ⓪ and four sidewall faces numbered as ①, ②, ③, and ④, respectively. The coordinate scope of those unloading faces, which are denoted by Γ_0, Γ_1, Γ_2, Γ_3 and Γ_4, respectively, are listed as

$$\left.\begin{aligned}
&\Gamma_0: \ x \in (-B/2 \sim B/2),\ y \in (-L/2 \sim L/2),\ z = H;\\
&\Gamma_1: \ x = -B/2,\ y \in (-L/2 \sim L/2),\ z \in (0 \sim H);\\
&\Gamma_2: \ x = B/2,\ y \in (-L/2 \sim L/2),\ z \in (0 \sim H);\\
&\Gamma_3: \ x \in (-B/2 \sim B/2),\ y = -L/2,\ z \in (0 \sim H);\\
&\Gamma_4: \ x \in (-B/2 \sim B/2),\ y = L/2,\ z \in (0 \sim H).
\end{aligned}\right\} \tag{1}$$

Assumptions are made for the analysis as follows: (1) the soil is assumed to be a homogenous and elastic solid medium; (2) the underlying tunnel is assumed to be an Euler–Bernoulli beam, and the deflection between the

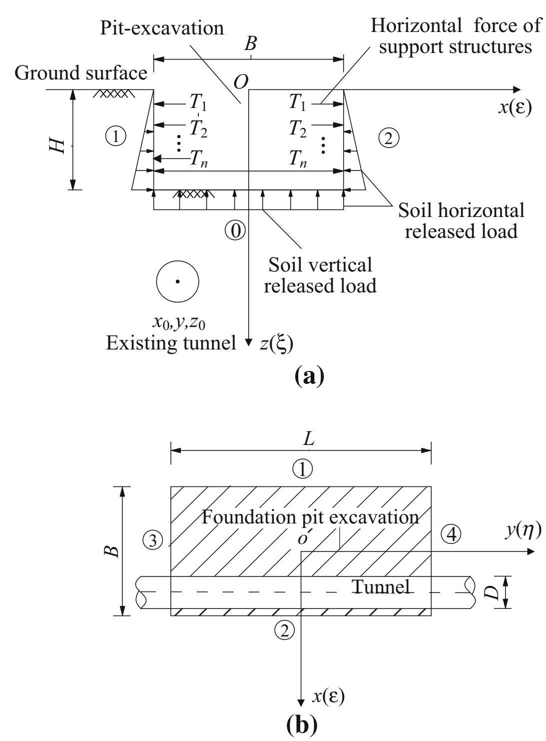

Fig. 1 Sketch of analytical model. **a** Front view. **b** Plan view

tunnel and surrounding soil is compatible; and (3) the tunnel is much longer comparing to the tunnel diameter, the influence of tunnel cross section is ignored.

2.2 Equivalent released load on the tunnel due to the excavation

The tunnel deflection is caused by the released load in vertical direction as being discussed in Sect. 3. As mentioned previously, the release load comes not only from the vertical unloading at the pit bottom, but also from the horizontal unloading and contribution of support structures on the pit sidewalls.

2.2.1 Equivalent released load caused by the vertical unloading at the pit bottom

Before excavation, there is a vertical stress distributing at the pit bottom, which can be calculated as γH, where γ is the unit weight of soil. Obviously, the excavation load acting on the pit bottom P in the opposite direction is equal to γH.

By employing Mindlin' solution [9], the vertical stress at the tunnel (i.e., the equivalent released load on the tunnel) should be

$$\begin{aligned}\sigma_z^{(0)}(x_0,y,z_0) &= \iint_{\Gamma_0} \frac{P}{8\pi}\left\{\upsilon_1\cdot\left(\frac{z_0-H}{R_1^3}-\frac{z_0-H}{R_2^3}\right)+\upsilon_2\cdot\frac{3z_0(z_0+H)^2}{R_2^5}\right.\\ &\quad+\upsilon_3\left[\frac{3(z_0-H)^3}{R_1^5}-\frac{3H(z_0+H)(5z_0-H)}{R_2^5}\right.\\ &\quad\left.\left.+\frac{30Hz_0(z_0+H)^3}{R_2^7}\right]\right\}\mathrm{d}\varepsilon\,\mathrm{d}\eta, \end{aligned} \tag{2}$$

where $\sigma_z^{(0)}(x_0,y,z_0)$ is the vertical stress at the tunnel with coordinates of (x_0, y, z_0); υ is the Poisson's ratio of soil; υ_1, υ_2, and υ_3 are constants given by $\upsilon_1=(1-2\upsilon)/(1-\upsilon)$, $\upsilon_2=(3-4\upsilon)/(1-\upsilon)$, and $\upsilon_3=1/(1-\upsilon)$, respectively; variables R_1 and R_2 are

$$\left.\begin{aligned} R_1&=\sqrt{(x-\varepsilon)^2+(y-\eta)^2+(z-H)^2},\\ R_2&=\sqrt{(x-\varepsilon)^2+(y-\eta)^2+(z+H)^2}, \end{aligned}\right\} \tag{3}$$

where (ε,η,H) is the coordinates of points at the bottom of the pit.

2.2.2 Equivalent released load caused by horizontal unloading and supports on the pit sidewalls

The horizontal unloading on the sidewalls of the pit depends on the interaction of the soil with the retaining walls and lateral braces. The incremental method can be adopted to analyze the support effect on the sidewalls of the pit, using the computational model as shown in Fig. 2.

Before excavation as shown in Fig. 2a, the soil pressure at the retaining wall can be computed as $K_0\gamma H$, where K_0 is the lateral pressure coefficient.

The excavation of the pit is usually from top to bottom in several steps and the depth of each step is h_i. According to the theory of incremental method [10, 11], there will be three parts of incremental loads acting on the retaining wall at each step including the incremental soil load, the incremental spring load, and the support prestressing load.

(1) The incremental soil load $\Delta q^{(n)}$ which is induced by the previous step excavation, can be expressed as

$$\Delta q^{(n)}=\begin{cases}\gamma(z-h^{(n-1)})K_0 & (h^{(n-1)}\le z\le h^{(n)})\\ \gamma(h^{(n)}-h^{(n-1)})K_0 & (z\ge h^{(n)})\end{cases}, \tag{4}$$

where the superscript n denotes the step n, $h^{(n-1)}$, and $h^{(n)}$ are the excavation depths at the previous step and current step, respectively. The load $\Delta q^{(n)}$ can be converted to a load vector $\Delta\boldsymbol{q}^{(n)}$ using one-dimensional finite element modeling.

(2) The incremental spring load $\boldsymbol{f}^{(n)}$, which is induced by the current step excavation (equivalent to elimination of the springs), can be expressed as,

$$\boldsymbol{f}^{(n)}=\boldsymbol{K}_{\mathrm{s1}}^{(n)}\cdot\Delta\boldsymbol{\delta}^{(n-1)}, \tag{5}$$

where $\boldsymbol{K}_{\mathrm{s1}}^{(n)}$ is the stiffness matrix of eliminated springs at the current step, and $\Delta\boldsymbol{\delta}^{(n-1)}$ is the displacement of retaining wall at the previous step.

(3) The support prestressing load $\boldsymbol{T}^{(n)}$ is induced by the prestressing force being applied to the lateral braces.

The three parts of the incremental load above are applied to the retaining wall, lateral braces, and remaining springs. Therefore, the finite element equation can be expressed as

$$(\boldsymbol{K}_{\mathrm{s2}}^{(n)}+\boldsymbol{K}_{\mathrm{r}}^{(n)}+\boldsymbol{K}_{\mathrm{b}}^{(n-1)})\cdot\Delta\boldsymbol{\delta}^{(n)}=\Delta\boldsymbol{q}_0^{(n)}+\boldsymbol{f}^{(n)}+\boldsymbol{T}^{(n)}, \tag{6}$$

where $\boldsymbol{K}_{\mathrm{s2}}^{(n)}$, $\boldsymbol{K}_{\mathrm{r}}^{(n)}$, and $\boldsymbol{K}_{\mathrm{b}}^{(n-1)}$ are the stiffness matrix of remaining springs at current step, the stiffness matrix of retaining wall at current step, and the stiffness matrix of lateral braces at previous step, respectively.

Since Eq. (6) is so complicated to solve theoretically, a computing program has been developed based on the finite

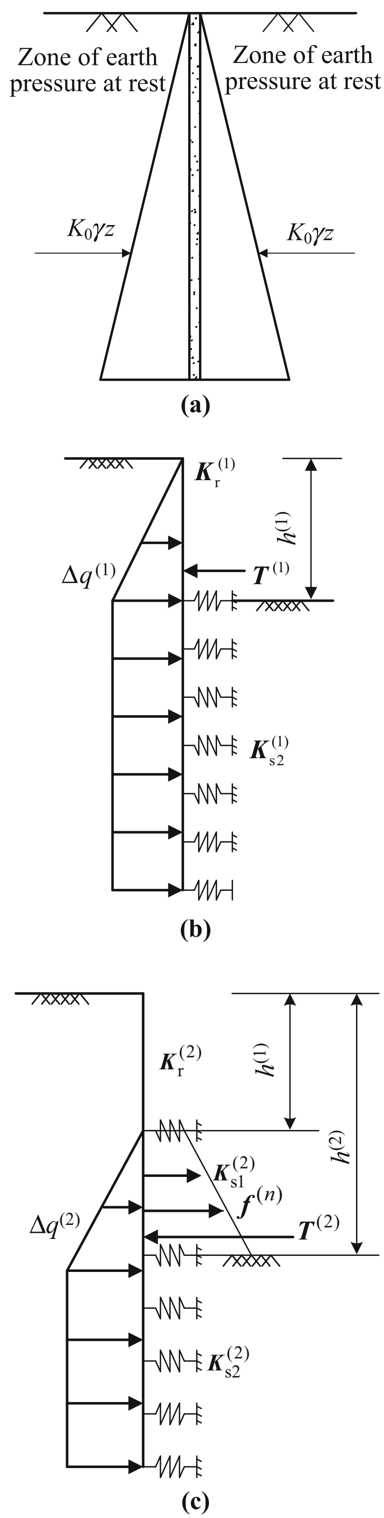

Fig. 2 Computational model. **a** Before excavation. **b** Excavation of the first bench. **c** Excavation of the second bench

element theory in order to solve Eq. (6). Once the pit is excavated up to the pit bottom, the final displacement of the retaining wall can be calculated as

$$\boldsymbol{\delta} = \sum_{n=1}^{N_{\mathrm{s}}} \Delta\boldsymbol{\delta}^{(n)}, \tag{7}$$

where N_{s} is number of excavation steps.

The horizontal released load of soil mass on the sidewall of the pit, $\boldsymbol{Q}_{\mathrm{s}}$, can be calculated as

$$\boldsymbol{Q}_{\mathrm{s}} = \sum_{n=1}^{N_{\mathrm{s}}} \Delta\boldsymbol{q}^{(n)}. \tag{8}$$

Due to the interaction of the retaining wall and soil, the horizontal support force provided by the retaining wall, $\boldsymbol{Q}_{\mathrm{r}}$, can be calculated as

$$\boldsymbol{Q}_{\mathrm{r}} = \boldsymbol{K}_{\mathrm{r}}^{(N_{\mathrm{s}})} \cdot \boldsymbol{\delta}. \tag{9}$$

Similarly, the horizontal support force provided by the ith lateral brace, $Q_{\mathrm{b}i}$, can be calculated as

$$Q_{\mathrm{b}i} = E_i A_i \delta_i, \tag{10}$$

where E_iA_i is stiffness of the ith lateral brace, and δ_i is horizontal displacement of the ith lateral brace.

The vectors $\boldsymbol{Q}_{\mathrm{s}}$ and $\boldsymbol{Q}_{\mathrm{r}}$ can be fitted as a continuous function of Q_{s} and Q_{r} using the spline function fitting method. Based on the above, the horizontal released load and horizontal support force of retaining wall, Q_{rs}, can be expressed as

$$Q_{\mathrm{rs}} = Q_{\mathrm{s}} + Q_{\mathrm{r}}. \tag{11}$$

Based on the Mindlin' solution, the vertical stress at the tunnel level induced by both horizontal released load and horizontal support force of retaining wall on sidewall ① of the pit, $\sigma_{\mathrm{zsr}}^{(1)}$, can be integrated as

$$\begin{aligned}\sigma_{\mathrm{zsr}}^{(1)}(x_0, y, z_0) = \iint_{\Gamma_1} \frac{Q_{\mathrm{rs}}(x_0-\varepsilon)}{8\pi} \\ \times \left\{ \upsilon_1 \cdot \left(\frac{-1}{R_1^3} + \frac{1}{R_2^3} - \frac{6\xi(z_0+H)}{R_2^5} \right) + 3\upsilon_2 \cdot \frac{(z_0+H)^2}{R_2^5} \right. \\ \left. + \upsilon_3 \left[\frac{3(z_0-H)^2}{R_1^5} - \frac{6\xi^2}{R_2^5} - \frac{30\xi z_0 (z_0+H)^2}{R_2^7} \right] \right\} \mathrm{d}\eta \, \mathrm{d}\xi,\end{aligned} \tag{12}$$

where ξ is the Z-coordinates of points on the pit sidewalls.

Similarly, the vertical stress at the tunnel level induced by horizontal force of lateral braces on the sidewall ① of the pit, $\sigma_{\mathrm{zb}}^{(1)}$, can be expressed as

$$\sigma_{z\mathrm{b}}^{(1)}(x_0,y,z_0)=\sum_{i=1}^{N_\mathrm{b}}\frac{Q_{\mathrm{b}i}(x_0-\varepsilon_i)}{8\pi}\times\left\{\upsilon_1\cdot\left(\frac{-1}{R_{1i}^3}+\frac{1}{R_{2i}^3}-\frac{6\xi(z_0+H)}{R_{2i}^5}\right)+3\upsilon_2\cdot\frac{(z_0+H)^2}{R_{2i}^5}+\upsilon_3\cdot\left[\frac{3(z_0-H)^2}{R_{1i}^5}-\frac{6\xi^2}{R_{2i}^5}-\frac{30\xi z_0(z_0+H)^2}{R_{2i}^7}\right]\right\}, \tag{13}$$

where N_b is number of lateral braces located at sidewall ①; Variables R_{1i} and R_{2i} are

$$\left.\begin{aligned}R_{1i}&=\sqrt{(x-\varepsilon_i)^2+(y-\eta_i)^2+(z-\xi_i)^2},\\R_{2i}&=\sqrt{(x-\varepsilon_i)^2+(y-\eta_i)^2+(z+\xi_i)^2},\end{aligned}\right\} \tag{14}$$

where $(\varepsilon_i,\eta_i,\xi_i)$ is the coordinates of lateral braces on the sidewall of the pit.

Therefore, the equivalent released load on the tunnel axis induced by the horizontal released load and horizontal support force (including retaining walls and lateral braces) on the sidewall ①, $\sigma_z^{(1)}(x_0,y,z_0)$, can be superimposed as

$$\sigma_z^{(1)}(x_0,y,z_0)=\sigma_{z\mathrm{sr}}^{(1)}(x_0,y,z_0)+\sigma_{z\mathrm{b}}^{(1)}(x_0,y,z_0). \tag{15}$$

Similarly, the equivalent released load on the tunnel axis induced by the horizontal released load and horizontal support force on the sidewalls ②, ③, and ④ can be derived as $\sigma_z^{(2)}(x_0,y,z_0)$, $\sigma_z^{(3)}(x_0,y,z_0)$, and $\sigma_z^{(4)}(x_0,y,z_0)$, respectively.

Based on the superposition principle, the equivalent released load at the tunnel level, $\sigma_z(x_0,y,z_0)$, can be obtained from

$$\sigma_z(x_0,y,z_0)=\sum_{i=0}^{4}\sigma_z^{(i)}(x_0,y,z_0). \tag{16}$$

2.3 Tunnel uplift due to the pit excavation

The unloading due to the pit excavation causes uplift $w(y)$ in the longitudinal direction of the existing tunnel below the pit, as shown in Fig. 3a.

In order to estimate the response of the existing tunnel to the equivalent released load, the tunnel is assumed to be a continuous and slender beam on an elastic foundation. To obtain a more accurate and rational result, an elastic Pasternak foundation model is adopted to simulate the interaction between the tunnel and surrounding soil as shown in Fig. 3b. The Pasternak foundation is improved from the traditional Winkler foundation by adding a layer of shear units on the foundation [12]. It can not only reflect the elastic deflection of the tunnel, but also embody the continuity of the soil.

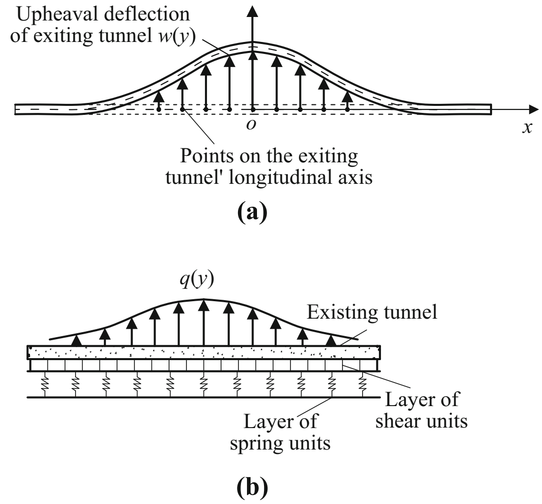

Fig. 3 Uplift of the existing tunnel in longitudinal axis (**a**) and Pasternak's foundation model (**b**)

2.3.1 *Differential equations of equilibrium*

As shown in Fig. 4, the external loads acting on the tunnel include two parts: one is the load $q(y)$ coming from the equivalent released load, which can be expressed as

$$q(y)=D\cdot\sigma_z(x_0,y,z_0), \tag{17}$$

where D is the tunnel diameter.

The other is the interaction load $p(y)$ coming from the shear units and spring units in the Pasternak model, which can be expressed as

$$p(y)=G\frac{\mathrm{d}^2w(y)}{\mathrm{d}y^2}-Kw(y), \tag{18}$$

where G is the foundation shear modulus, K is the bulk modulus, and $w(y)$ is the uplift along the tunnel axis.

To obtain the equilibrium differential equation subjected to the external loads on the Pasternak' foundation, the balance mechanism of a beam unit can be described as shown in Fig. 5.

The force balance condition of $\Sigma Y=0$ for the beam unit can be written as

$$Q-(Q+\mathrm{d}Q)+q(y)\mathrm{d}y-p(y)\mathrm{d}y=0, \tag{19}$$

where Q is the shearing force of Z-axis direction.

Equation (19) can be simplified as

$$\frac{\mathrm{d}Q}{\mathrm{d}y}=q(y)-p(y). \tag{20}$$

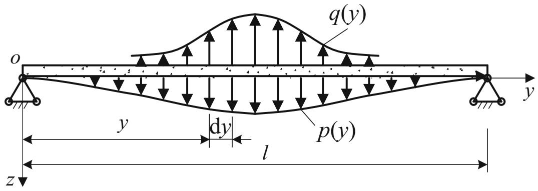

Fig. 4 External loads acting on the tunnel

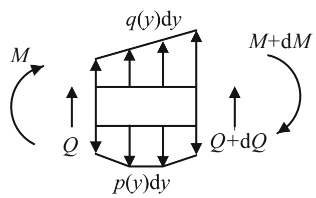

Fig. 5 The balance mechanism of a beam unit

The force balance condition of $\Sigma M = 0$ for the beam unit can be written as

$$M-(M+\mathrm{d}M)+(Q+\mathrm{d}Q)\mathrm{d}y+q(y)\frac{(\mathrm{d}y)^2}{2}-p(y)\frac{(\mathrm{d}y)^2}{2}=0, \tag{21}$$

where M is the bending moments of Y-axis direction.

Given that the second trace can be omitted, Eq. (21) is simplified as

$$Q=\frac{\mathrm{d}M}{\mathrm{d}y}. \tag{22}$$

Taking the derivative of Eq. (22) to get an expression as

$$\frac{\mathrm{d}Q}{\mathrm{d}y}=\frac{\mathrm{d}^2M}{\mathrm{d}y^2}, \tag{23}$$

according to Eqs. (20) and (23), a relationship can be obtained as

$$\frac{\mathrm{d}^2M}{\mathrm{d}y^2}=q(y)-p(y). \tag{24}$$

By substituting Eqs. (17) and (18) into Eq. (24), we obtain the displacement balance equation as follows:

$$\frac{\mathrm{d}^2M}{\mathrm{d}y^2}-G\frac{\mathrm{d}^2w(y)}{\mathrm{d}y^2}+Kw(y)=D\sigma_z(x_0,y,z_0). \tag{25}$$

Based on the material mechanics theory, the relationship between bending moment and displacement of the continuous beam can be expressed as

$$\frac{\mathrm{d}^2M}{\mathrm{d}y^2}=EI\frac{\mathrm{d}^4\mathrm{w(y)}}{\mathrm{d}y^4}, \tag{26}$$

where EI is the longitudinal bending stiffness of the tunnel. By substituting Eq. (26) into Eq. (25), the differential equations of equilibrium for the uplift of the tunnel can be obtained as

$$\frac{\mathrm{d}^4w(y)}{\mathrm{d}y^4}-\frac{GD}{EI}\frac{\mathrm{d}^2w(y)}{\mathrm{d}y^2}+\frac{DK}{EI}w(y)=\frac{q(y)}{EI}. \tag{27}$$

2.3.2 *The solution of the differential equation*

From Eq. (27), a fourth-order homogeneous differential equation corresponding to Eq. (27) can be written as

$$\frac{\mathrm{d}^4w(y)}{\mathrm{d}y^4}-\frac{GD}{EI}\frac{\mathrm{d}^2w(y)}{\mathrm{d}y^2}+\frac{DK}{EI}w(y)=0. \tag{28}$$

The characteristic equation of Eq. (28) is

$$r^4-\frac{GD}{EI}r^2+\frac{KD}{EI}=0. \tag{29}$$

The general solutions of Eq. (29) depend on $\varDelta$ which can be expressed as

$$\varDelta=\left(\frac{GD}{EI}\right)^2-\frac{4KD}{EI}. \tag{30}$$

(1) When $\varDelta>0$, the solutions of Eq. (29) are

$$r_{1,2}=\pm\sqrt{\frac{GD+\sqrt{(GD)^2-4kDEI}}{2EI}}=\pm\alpha, \tag{31}$$

$$r_{3,4}=\pm\sqrt{\frac{GD-\sqrt{(GD)^2-4kDEI}}{2EI}}=\pm\beta. \tag{32}$$

The general solution of Eq. (28) can be written as

$$w(y)=A_1\mathrm{e}^{\alpha y}+A_2\mathrm{e}^{-\alpha y}+B_1\mathrm{e}^{\beta y}-B_1\mathrm{e}^{\beta y}. \tag{33}$$

(2) When $\varDelta=0$, the solutions of Eq. (29) are

$$r_{1,2}=\sqrt{\frac{GD}{2EI}}=\alpha,\quad r_{3,4}=-\sqrt{\frac{GD}{2EI}}=-\alpha. \tag{34}$$

The general solution of Eq. (28) can be written as

$$w(y)=(A_1+A_2)\mathrm{e}^{\alpha y}+(B_1+B_2)\mathrm{e}^{\beta y}. \tag{35}$$

(3) When $\varDelta<0$, the solutions of Eq. (29) are

$$r_{1,2,3,4}=\pm\sqrt{\sqrt{\frac{KD}{4EI}}+\frac{GD}{4EI}}\pm\sqrt{\sqrt{\frac{KD}{4EI}}-\frac{GD}{4EI}}\cdot i=\pm\alpha\pm\beta. \tag{36}$$

The general solution of Eq. (28) can be written as

$$w(y) = [A_1\cos(\beta y) + A_2\sin(\beta y)]\cdot e^{\alpha y} + [B_1\cos(\beta y) + B_2\sin(\beta y)]\cdot e^{-\alpha y}. \tag{37}$$

Assuming that there is a concentrated load acting on the tunnel, when y tends to be infinity, the value of $w(y)$ will tend to be zero, so, the expression of $w(y)$ can be simplified as,

$$w(y) = \begin{cases} A_1 e^{-\alpha y} + A_2 e^{-\beta y} & \Delta > 0, \\ (A_1 + A_2 y)e^{-\alpha y} & \Delta = 0, \\ [A_1\cos(\beta y) + A_2\sin(\beta y)]e^{-\alpha y} & \Delta < 0. \end{cases} \tag{38}$$

The continuously distributed load $q(y)$ is divided into many concentrate loads $q(y)\mathrm{d}y$ on segments of the tunnel. Then the boundary condition of the segment can be expressed as

$$\left.\begin{aligned} &\frac{\mathrm{d}w(y)}{\mathrm{d}y} = 0, \\ &EI\frac{\mathrm{d}^2 w(y)}{\mathrm{d}y^2} = \frac{q(y)\mathrm{d}y}{2}. \end{aligned}\right\} \tag{39}$$

According to the general solution Eq. (38) and boundary condition Eq. (39), the uplift of the tunnel induced by a concentrated load of $q(\eta)\mathrm{d}\eta$ can be derived as

$$\mathrm{d}w(y) = \begin{cases} \dfrac{q(\eta)D}{2EI\alpha\beta(\beta^2-\alpha^2)}(\beta e^{-\alpha|y-\eta|} - \alpha e^{-\beta|y-\eta|})\mathrm{d}\eta & \Delta > 0, \\ \dfrac{q(\eta)D}{4EI\alpha^3}(1+\alpha|y-\eta|)e^{-\alpha|y-\eta|}\mathrm{d}\eta & \Delta = 0, \\ \dfrac{q(\eta)D}{4EI\alpha\beta(\alpha^2+\beta^2)}e^{-\alpha|y-\eta|}[\beta\cos(\beta|y-\eta|) + \alpha\sin(\alpha|y-\eta|)]\mathrm{d}\eta & \Delta < 0. \end{cases} \tag{40}$$

Using the integration method, the uplift of the tunnel induced by the pit excavation can be obtained from Eq. (40) as

$$w(y) = \int_{-\infty}^{\infty} \mathrm{d}w(y)\mathrm{d}\eta. \tag{41}$$

3 A case study for validation

The approach described above is applied to an actual project case, and the analytical result is compared with the results obtained from numerical modeling and monitoring for validating the approach.

Table 1 Geotechnical properties

Soil name	H (m)	γ (kN/m^3)	c (kPa)	φ(°)	E_s (MPa)	υ
Backfill	2.1	19.0	12	18.0	17.0	0.4
Sandy clay	5.2	18.5	18	0.0	24	0.3
Gravelly clay	16.8	19.5	22	20.0	22	0.3
Weathered red granite	15.0	22.0	30	35.0	41.38	0.3

3.1 Background of the project

The net horizontal distance between the double-hole subway tunnels is 12.0 m. The outside diameter of the subway tunnel is 6.2 m and the thickness of tunnel lining is 0.35 m. The net vertical distance from the bottom of open-cut pit to the crown of the tunnels is 11.5 m. The net horizontal distance between the pit center and the right subway tunnel is 6.9 m.

The soil encountered in the project consists of saturated cohesive sandy and gravelly clay. The geotechnical properties are listed in Table 1, where c is the cohesive force of soil, φ the friction angle of soil, and E_s the compression modulus of soil layer.

The open-cut pit is supported by retaining walls and lateral braces where the retaining walls are constructed from bored piles and the lateral braces use steel pipes.

3.2 Analytical calculation

A theoretical analysis is carried out to calculate the uplift of the tunnel using the analytical solution presented above. The calculation parameters employed in the analytical calculation is determined as follows.

3.2.1 Soil parameters

The layered soils are combined as a homogenous soil layer. The soil density γ and Poisson's ratio υ are from the weighted average of γ_i and υ_i of layered soils. The elastic modulus of E is determined according to the compressibility modulus from the following formula [13] as

$$E = \frac{E_s^*(1+\upsilon)(1-2\upsilon)}{(1-\upsilon)}, \tag{42}$$

where E_s^* is the weighted average of compressibility modulus of layered soils.

(2) Foundation parameters.

The Simply Elastic Space Method proposed by Kerr [14] is employed to determine the foundation parameters of K and G from the following formula

$$K = E/H', \quad G = \frac{GH'}{3} = \frac{E}{2(1+\upsilon)} \cdot \frac{H'}{3}, \tag{43}$$

where H' is the thickness of the foundation soil, and can be calculated by $H' = 6D$ according to Zhang [7].

(3) Longitudinal bending stiffness of the tunnels.

The subway tunnel constructed by the shield-driven method is assembled by segment rings which are connected with high-strength bolts. Thus, the longitudinal bending stiffness of the subway tunnel can be considered as a stiffness reduced from a tubular structure and expressed as

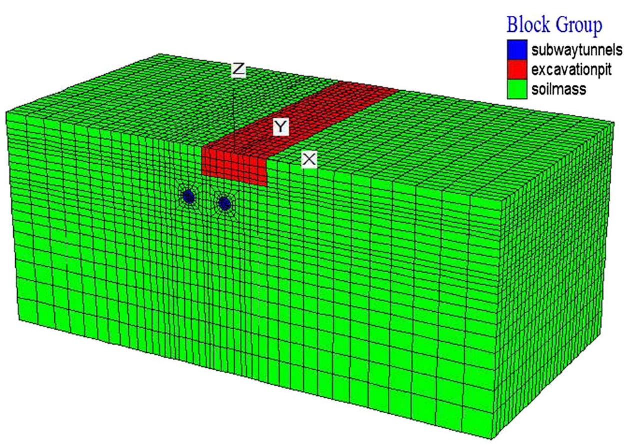

Fig. 6 The computational model

$$EI = \eta E_c I_c, \tag{44}$$

where η (between 1/5 and 1/7) is the equivalent reduction coefficient of tunnel' bending stiffness [15], E_c is the modulus of reinforced concrete, and I_c is the inertia moment of the tunnel. Based on the above, an analytical result is obtained as shown in Fig. 7.

3.3 Numerical modeling

A 3D numerical modeling for the soil-structure interaction is conducted. Figure 6 is the computational model. The model consists of 34,410 nodes and 31,350 elements.

To be comparable with the analytical solution, the elastic constitutive model is used to simulate the soil. The shell element is used to simulate the tunnel concrete lining that is classified as grade C55, and the beam element is used to simulate the support structure including bored piles of retaining wall and steel pipes of lateral braces.

The material properties are summarized in Table 2, where K_s is the bulk modulus of the soil, u is the lateral pressure coefficient of the soil, I_p is the sectional moment of inertia, and A_s is the cross-sectional area of the support structures.

3.4 Results comparison

During the pit construction, the uplift of the existing subway tunnels is monitored. Figure 7 shows the comparison of the analytical solution with the numerical modeling and monitoring results.

From Fig. 7, it can be seen that the analytical solution agrees well with the numerical modeling and monitoring result, which in turn validated the analytical solution proposed in this study. The maximum uplift occurs at the pit center, and the uplift of the right-line tunnel is bigger than that of the left-line tunnel. It is demonstrated that the closer the tunnel is to the pit, the greater the disturbance of excavation on the adjacent tunnel.

By adopting the common uplift criterion of 0.50 mm, it can be seen from Fig. 7 that the influence of the pit

Table 2 Material parameters

Soil	γ (kg·m^{-3})	K_s (GPa)	υ	u	
	1,930.0	0.7	0.3	2.1	
Tunnel lining	P (kg·m^{-3})	E (GPa)	υ	EI (KN·m^2)	η
	2,500.0	34.5	0.2	2.8×10^7	1.7×10^{-1}
Bored piles supporting	γ (kg·m^{-3})	E (GPa)	υ	I_p (m^3)	A_s (m^2)
	2,400.0	30.0	0.2	4.9×10^{-2}	0.8
Steel pipe supporting	γ (kg·m^{-3})	E (GPa)	υ	I_p (m^3)	A_s (m^2)
	2,400.0	210.0	0.2	3.6×10^{-4}	1.5×10^{-2}

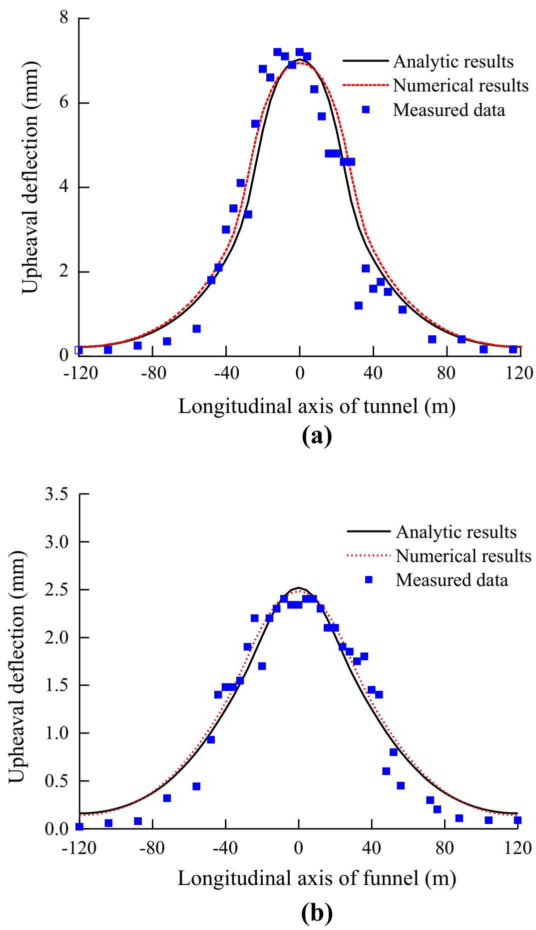

Fig. 7 Uplift deflection of double-hole subway tunnels along the tunnel axis. **a** Right line. **b** Left line

excavation on the existing tunnel is about 240.00 m, which is equivalent to 6 times the pit excavation length. The maximum uplifting of the double-hole subway tunnel is 7.20 mm at the right line and 2.34 mm at the left line, both are within the allowable deflection of 10.00 mm, which indicates that the subway tunnel would be safe.

4 A parametric study

In order to investigate the influence of various factors on the tunnel deflection, a parametric study is carried out. A hypothetical pit excavation is adopted in this study with an excavation depth of 8.0 m. The length and width of the excavation are L and B, respectively, as shown in Fig. 8. The single existing tunnel with a diameter of 6.0 m is parallel to the pit. The vertical distance between the excavation bottom and the tunnel axis is denoted as d_1, and the horizontal distance from the excavation center to the tunnel axis is d_2. The soil is assumed to be continuous and homogeneous. The tunnel length is 240.0 m. The density, elastic modulus, and Poisson's ratio of the soil are 18.5 kN/m^3,

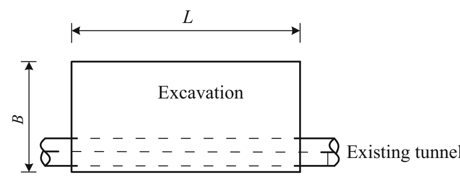

Fig. 8 The excavation size

260.0 MPa and 0.3, respectively. The longitudinal bending stiffness of the tunnel is 122,650.0 MN·m^2.

4.1 Influence of the excavation size

4.1.1 Effect of excavation length

Five cases of excavation length L (20.0, 30.0, 40.0, 50.0, and 60.0 m) are used to examine the effect of the excavation length on the tunnel. Other factors of B, d_1, and d_2 are assumed as 10.0, 8.0, and 0.0 m, respectively. Figure 9a shows the uplift of the tunnel along the longitudinal axis for various L. It can be seen that the maximum uplift increases with the increasing L in a nonlinear manner.

4.1.2 Effect of excavation width

Five cases of excavation width B (10.0, 20.0, 30.0, 40.0, and 50.0 m) are used to examine the effect of the excavation width on the tunnel. Other factors of L, d_1, and d_2 are assumed as 20.0, 8.0, and 0.0 m, respectively. Figure 9b shows the uplift of the tunnel along the longitudinal axis for various B. As shown in Fig. 9b, the uplift and influential range of tunnel's deflection increases with the excavation width.

It can be seen from Fig. 9 that the excavation size has a significant influence on the tunnel. Furthermore, the effect of the excavation width on the tunnel is bigger than that of the length.

4.2 Influence of the relative distances

The relative distance from the pit excavation to the tunnel includes the vertical distance d_1 and horizontal distance d_2 as shown in Fig. 10.

4.2.1 Effect of the vertical distance

Five cases of vertical distance d_1 (6.0, 8.0, 10.0, 12.0, and 14.0 m) are used to examine the effect of vertical distance. Other factors of L, B, and d_2 are assumed to be 20.0, 10.0, and 0.0 m, respectively. Figure 11a shows the uplift of the tunnel along the longitudinal axis for various d_1. It can be seen that the maximum uplift decreases from 2.68 mm to 2.04 mm when the vertical distance increases from 6.0 m to 14.0 m,

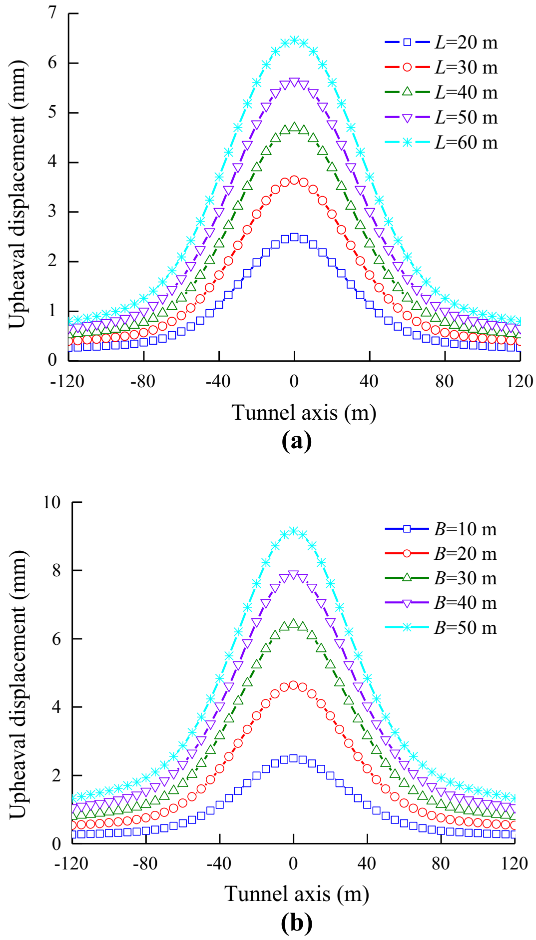

Fig. 9 A parametric study on excavation size. **a** Effect of the excavation length L ($B = 10$ m). **b** Effect of the excavation width B ($L = 20$ m)

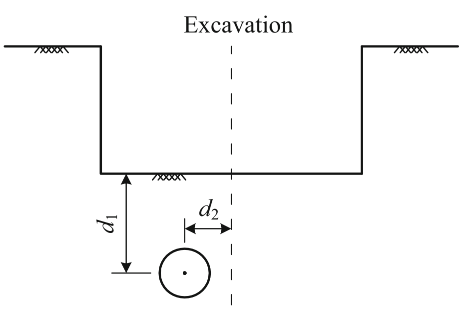

Fig. 10 The relative distance

which indicates that the effect of vertical distance reduces along with the excavation moving away from the tunnel.

4.2.2 *Effect of horizontal distance*

Five cases of horizontal distance d_2 (0.0, 2.0, 4.0, 6.0, and 8.0 m) are used to examine the effect of horizontal

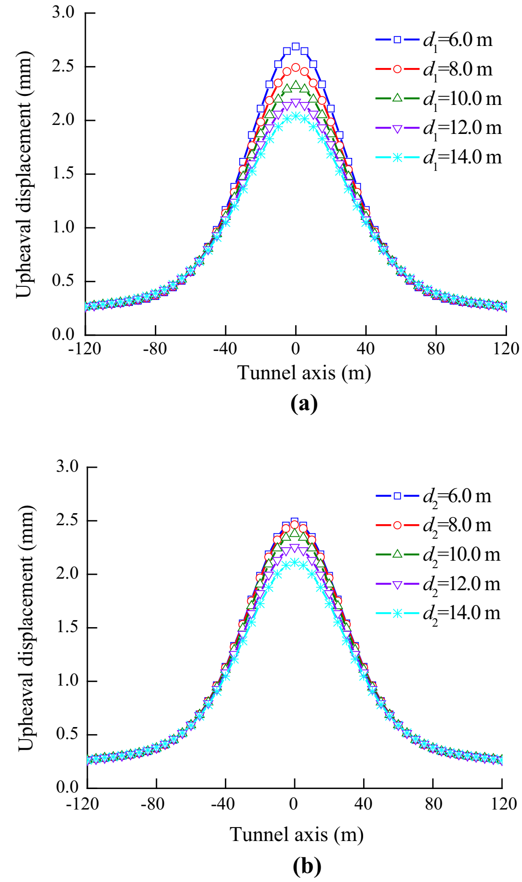

Fig. 11 Parametric study on relative distance. **a** Effect of the vertical distance d_1 ($d_2 = 0.0$ m). **b** Effect of the horizontal distance d_2 ($d_1 = 8.0$ m)

distance. Other factors of L, B, and d_1 are assumed to be 20.0, 10.0, and 8.0 m, respectively. Figure 11b shows the uplift of the tunnel along with longitudinal axis for different d_2. It can be seen that the maximum uplift of the tunnel is 2.49 mm when the horizontal distance is $d_2 = 0.0$ m, while it is 2.11 mm when the horizontal distance is $d_2 = 8.0$ m. This indicates that the vertical distance has a bigger influence on the tunnel than that of the horizontal distance.

From Fig. 11, it can be seen that the influential range is almost the same at various relative distances, which indicates that the relative distance affects only the uplift, but not the influenced range.

5 Conclusion

From this study, some useful conclusions may be dawn as follows:

(1) An analytical approach based on the principle of two-stage method and incremental method is proposed to

estimate the deflection of subway tunnels induced by adjacent excavations. By comparing with numerical modeling and monitoring results, it can be concluded that the proposed approach is effective and reliable.

(2) In the proposed approach, an elastic Pasternak model is adopted to describe the response of the existing tunnel to the excavation-induced released loads. As the Pasternak model can take account of shearing, it can provide a more accurate and rational result than the traditional model of Winkler foundation.

(3) It is found that the influential range on the tunnel is about 6 times the length of the pit excavation.

(4) From the parametric study, it is found that the uplift of the tunnel due to adjacent excavations increases with the excavation size and decreases with the relative distance. The excavation size has a significant effect on both uplift and influential range, while the relative distance impacts only the uplift of the tunnel, but not the influential range.

Acknowledgments The research is supported by the Fundamental Research for the Central Universities (SWJTU11ZT33) and the Funds for the development of Innovation team of Ministry of Education (IRT0955).

References

1. Chang CT, Sun CW, Duann SW, Hwang RN (2001) Response of a Taipei rapid transit system (TRTS) tunnel to adjacent excavation. Tunn Undergr Sp Technol 16(3):151–158
2. Dolezalova M (2001) Tunnel complex unloaded by a deep excavation. Comput Geotech 28(3):469–493
3. Gao GY, Gao M, Yang CB, Yu ZS (2010) Influence of deep excavation on deformation of operating metro tunnels and countermeasures. Chin J Geotech Eng 32(3):453–459
4. Hu ZF, Yue ZQ, Zhou J, Tham LG (2003) Design and construction of a deep excavation in soft soils adjacent to the Shanghai Metro tunnels. Can Geotech J 40(5):933–948
5. Ji MJ, Liu GB (2001) Prediction method of displacement of subway tunnel due to excavation. J Tongji Univ 29(5):531–535
6. Zhang ZG, Zhang MX, Wang WD (2011) Two-stage method for analyzing effects on adjacent metro tunnels due to foundation pit excavation. Rock Soil Mech 32(7):2085–2092
7. Zhang H, Zhang ZX (2013) Vertical deflection of existed pipeline due to shield tunneling. J Tongji Univ (Nat Sci) 41(8):1172–1178
8. Huang X, Huang HW, Zhang DM (2012) Longitudinal deflection of existing shield tunnels due to deep excavation. Chin J Geotech Eng 34(7):1241–1249
9. Mindlin RD (1936) Force at a point in the interior of a semi-infinite solid. Physics 7(1):195–202
10. Feng SJ, Chen XX, Gao GY, Zhang JX (2009) Analysis of underground diaphragm wall by iterative incremental method. Rock Soil Mech 30(1):226–230
11. Yang GH (2004) Practical calculation method of retaining structures for deep excavations and its application. Rock Soil Mech 12:1885–1896 + 1902
12. Pasternak PL (1954) On a new method of analysis of an elastic foundation by means of two-constants. State Architecture & construction Press, Moscow
13. Yin DS, Wang BT (2007) Test and modulus formula for lateral unloading and loading stress paths during excavation in foundation pit. Rock Soil Mech 28(11):2421–2425
14. Kerr AD (1985) On the determination of foundation model parameters. J Geotech Eng 111(11):1334–1340
15. Zhang DM, Zong X, Huang HW (2014) Longitudinal deformation of existing tunnel due to underlying shield tunneling. Rock Soil Mech 35(9):2659–2666